An Adhesive Peptide from the C-Terminal Domain of α-Synuclein for Single-Layer Adsorption of Nanoparticles onto Substrates

Ghibom Bhak, Alejandro Mendez-Ardoy, Albert Escobedo, Xavier Salvatella, and Javier Montenegro

Accepted Manuscript

How to cite:

Bioconjugate Chem. 2020, 31, 12, 2759–2766

An Adhesive Peptide From the C-Terminal Domain of α-Synuclein for Single-layer Adsorption of Nanoparticles onto Substrates

Ghibom Bhak[1], Alejandro Méndez-Ardoy[1], Albert Escobedo[2,3], Xavier Salvatella[2,3,4] and Javier Montenegro[1]*

[1]Centro Singular de Investigación en Química Biolóxica e Materiais Moleculares (CIQUS), Departamento de Química Orgánica, Universidade de Santiago de Compostela, 15782 Santiago de Compostela, Spain

[2]Institute for Research in Biomedicine (IRB Barcelona), The Barcelona Institute of Science and Technology, Baldiri Reixac 10, 08028 Barcelona, Spain.

[3]Joint BSC-IRB Research Programme in Computational Biology, Baldiri Reixac 10, 08028 Barcelona, Spain.

[4]ICREA, Passeig Lluís Companys 23, 08010 Barcelona, Spain.

KEYWORDS. peptides · biomaterials · nanoparticles · surface adhesion.

ABSTRACT: The two-dimensional (2D) homogenous assembly of nanoparticle monolayer arrays onto a broad range of substrates constitutes an important challenge for chemistry, nanotechnology and material science. α-Synuclein (αS) is an intrinsically disordered protein associated with neuronal protein complexes and has a high degree of structural plasticity and chaperone activity. The C-terminal domain of αS has been linked to the non-covalent interactions of this protein with biological targets and the activity of αS in pre-synaptic connections. Herein, we have systematically studied peptide fragments of the chaperone-active C-terminal sequence of αS and identified a 17-residue peptide that preserves the versatile binding nature of αS. Attachment of this short peptide to gold nanoparticles afforded colloidally stable nanoparticle suspensions that allowed the homogenous 2D adhesion of the conjugates onto a wide variety of surfaces, including the formation of crystalline nanoparticle superlattices. The peptide sequence and the strategy reported here describe a new adhesive molecule for the controlled monolayer adhesion of metal nanoparticles and sets a stepping-stone towards the potential application of the adhesive properties of αS.

Introduction

The controlled assembly of nanoparticles (NPs) onto surfaces of materials is of great importance to exploit their chemical and electrical properties. In particular, the two-dimensional (2D) organization of NP arrays on appropriate substrates is key for the fabrication of high-performance nanodevices for future optoelectronic, biosensing, and energy-harvesting applications.[1-5] Recently, different strategies have been explored to construct 2D NP arrays on various surfaces such as glass, metal, or carbon substrates by employing chemical, polymeric, or biomolecular linkers.[6-9] However, these methodologies have been restricted to particular types of substrates, which limit their widespread applications. Particularly for biomolecular linkers, DNA templates have been employed for the controlled positioning of metal NP networks and superlattices.[10,11] Additionally, proteins have emerged as a versatile alternative strategy to organize NP coatings.[12-16] Protein methodologies benefit from the control of molecular conformation afforded by fine-tuning external stimuli such as pH or ionic strength, to modulate the multivalent and non-covalent interactions of the conjugate with the substrate of interest.[13,17] Inspired by mussel proteins polydopamine scaffolds were shown to bind onto wide range of substrates[18] and find applications in lithium-ion batteries,[19] cell-culturing[20], and omnifluidic devices.[21] However, polydopamine mediated NP immobilization gave rise to heterogeneous surface absorption.[22,23] Recently, α-synuclein (αS) has been employed to functionalize gold nanoparticles (AuNPs)[24,25] and the resulting conjugates were employed as an adhesive composite for a wide range of substrates,[13] which showed excellent electronic, optical, and catalytic properties.[6]

αS is an intrinsically disordered protein of 140 residues that is abundant in presynaptic terminals[26] and has been implicated in the pathogenesis of neurodegenerative disorders such as Parkinson's disease.[27] αS promotes the assembly of the SNARE complex, in which the N-terminal domain of αS binds to synaptic vesicles, and the C-terminal region concurrently interacts with a vesicle-associated protein.[28] These multiple binding events are mainly attributed to the αS structural plasticity,[29,30] which has been shown to allow binding of the protein to multiple molecules,[29] and to interconvert between different structures depending on external conditions (i.e. pH, membrane interactions).[31] The primary structure of αS can be divided into three domains, a basic N-terminus (residues 1-60),[32] a hydrophobic central segment of non-amyloid-β component (NAC, residues 61-95),[33] and an acidic C-terminus domain (96-140).[34] The N-terminal domain forms amphipathic α-helices upon binding to lipid membranes through its seven imperfect 11-residue repeats.[35] The NAC segment has a high propensity to self-assemble and adopt a β-sheet conformation, leading to amyloid fibril formation.[33] In contrast, the C-terminal region, enriched in acidic residues (10 glutamates and 5 aspartates) maintains a disordered structure, thus participating in neither α-helices[36] nor β-sheets.[37] Yet, this highly anionic flexible C-terminal domain is responsible for αS thermosolubility,[38] chaperone activity[39-42] regulation of aggregation,[43,44] and multiple interactions with various mol-

ecules such as tau,[45] oxidized glutathione (GSSG),[46] phthalocyanine tetrasulfonate (PcTS),[47] eosin[48], and dequalinium (DQ),[49] among others.[50] This intriguing promiscuous binding to these different molecules has been shown to facilitate either the fibrillization[45-47] or oligomerization[48,49] of αS *in vitro*. Furthermore, the acidic C-terminus of αS results in pH-dependent behaviors such as accelerated self-assembly at low pH[51,52] and translocation to the cellular membrane upon intracellular acidification.[53] As previously mentioned, the identification of these stimuli responsive non-covalent interactions of αS has prompted new opportunities for the bio-conjugation of αS onto AuNP surfaces, resulting in hybrid materials with adhesive properties.[13] However, the inter-particle distance was limited to the hydrodynamic radius of the protein, which resulted in the formation of a thick organic layer between the surface adhered particles. Furthermore, the time-consuming and high-cost process required for the expression and purification of this intrinsically disordered protein restricted the design optimization and the potential applications of the technology. All in all, the binding mode of the αS to biomolecules suggested a potential adhesive functional role of the radially extended C-terminal domain of this intriguing protein.[13]

The C-terminal domain of αS includes a 16-residue sequence $_{125}$YEMPSEEGYQDYEPEA$_{140}$, which is crucial for the chaperone activity of αS.[42] The chaperone function has also been related to the structural plasticity of the C-terminal domain that allows the promiscuous binding to substrates.[54-56] In fact, removing the C-terminal domain leads to the loss of the chaperone activity of the αS protein.[42] Therefore, we hypothesized that this C-terminal sequence would constitute a peptide motif capable of mimicking the protein's adhesive behavior. Here we have systematically studied short anionic peptide sequences of the C-terminal domain and identified a 17 amino acids peptide sequence that retained the protein's adhesion capabilities without the synthetic and size limitations of the full length protein. The short peptide sequence allowed the straightforward and pH-controlled deposition of a tightly packed large-area single layer of AuNPs over a range of different material substrates. In addition, this peptide showed the potential crystalline adhesion of AuNPs on mica surfaces into close-contact superlattices, which has not yet been possible with any peptide-related biomaterial. The adhesive behavior was characterized in detail by scanning electron microscopy (SEM) and atomic force microscopy (AFM) in the presence of different substrates. The discovery of this new αS-derived peptide puts forward a new design strategy for the development of soft molecular binding peptides.

Results and Discussion

Adhesive Peptide Derived from C-terminal Domain of α-Synuclein (αS). A highly anionic 16-residue peptide (YEMPSEEGYQDYEPEA-NH_2; αSP) of the C-terminal domain of αS was chosen as initial peptide fragment due to its key role in protein chaperone activity and its potential involvement in the adhesive behavior of αS (Fig. 1a). Analysis of the peptide sequence revealed a 37.5% of enrichment in anionic (i.e. carboxylate) residues and a high content of hydrophobic/aromatic amino acids (43.75%), which would allow a high water-solubility in physiological conditions and could enhance non-covalent interactions (e.g. van der walls) with the surface after acidification. A series of truncated peptides and control sequences were also designed and prepared (see peptide nomenclature in Table S1). The peptide sequences were equipped with a N- or a C-terminal cysteine residue (αSP_N or αSP_C for parent peptide) for the attachment of the sequence to AuNPs (~ 20 nm) (Fig. 1b and 1c), which were used as a model target for the characterization of the potential adhesion properties (see supporting information). Rink amide solid phase peptide synthesis[57,58] was employed to prepare the different peptides capped with an amide group in the C-terminus, followed by HPLC purification and characterized by mass spectrometry and nuclear magnetic resonance (NMR) spectroscopy (Section S2.4, Fig. S25-32). To prepare the peptide/NP conjugates, AuNPs were incubated with the different peptides and the resulting conjugates were centrifuged, thoroughly washed with 20 mM MES (pH 6.5) and MilliQ water (three cycles) followed by re-suspension in aqueous buffer (Fig. 1). Following this protocol, the peptide/AuNP conjugates showed a well-dispersed colloidal state during all purification steps and after the final aqueous resuspension at neutral pH (Fig. S1). As shown by the gold plasmonic band and confirmed by a flocculation assay (Fig. S2), the colloidal suspensions were perfectly stable at neutral pH even at a high ionic strength (i.e. 1.25 M NaCl).

To investigate potential surface adhesion, the pH of these suspensions was acidified by re-suspension in 50 mM citrate buffer (pH = 4.5) and each colloidal solution was immediately placed onto a silicon wafer substrate (Fig. 1d). In order to ensure that the peptide-surface interactions controlled the adhesion process while minimizing potential defects in the resulting monolayer the incubation was performed for a sufficient time window of 3 hours. After incubation with the conjugates, the surface was thoroughly washed with 20% methanol and purged with N_2 (see supporting information). Incubation of the C-terminus-to-AuNP conjugates (αSP_C-AuNPs) onto the silicon wafer substrate resulted in disordered and amorphous aggregation of the particles on the surface (Fig 1c). By contrast, drop casting of the silicon surface with the N-terminus-to-AuNP conjugates (αSP_N-AuNP) showed smooth adsorption of AuNPs onto the surface, forming a high-density single layer coat (Fig 1b). The controlled acidification of the αSP_N-AuNPs dispersion (to pH 4.5) triggered the instantaneous adhesion of the particle monolayers onto the substrates and also onto the tip used for pipetting, which was immediately covered with a thin purple AuNP layer (Fig. S3). The silicon surfaces consequently showed a perfectly extended large-area single layer of αSP_N-AuNPs adsorbed on the silicon surface. Notably, the homogenous particle monolayer area could be extended as large as the conjugate droplet covering the surface and in the current study a 1-cm^2 sized surface was straightforwardly prepared (Fig. S4). Interestingly, while the acidified (pH 4.5) peptide/particle conjugates attached by the N-terminus (αSP_N-AuNPs) remained in colloidal state, the C-terminus functionalized particles (αSP_C-AuNPs) showed a much stronger aggregation and precipitation tendency at this pH after incubation at 40 °C, as revealed by naked eye observations and dynamic light scattering measurements (Fig. S5 and S6). It should be noted that the positioning of the N-terminal cationic ammonium moiety, located in the internal core of the N-terminal functionalized particles or in the external layer of the C-terminal conjugates, could impact the potential electrostatic interactions between particles after acidification. Nevertheless, the optimal N-terminal orientation of the peptide attached to the particles was consistent with the orientation of the αS

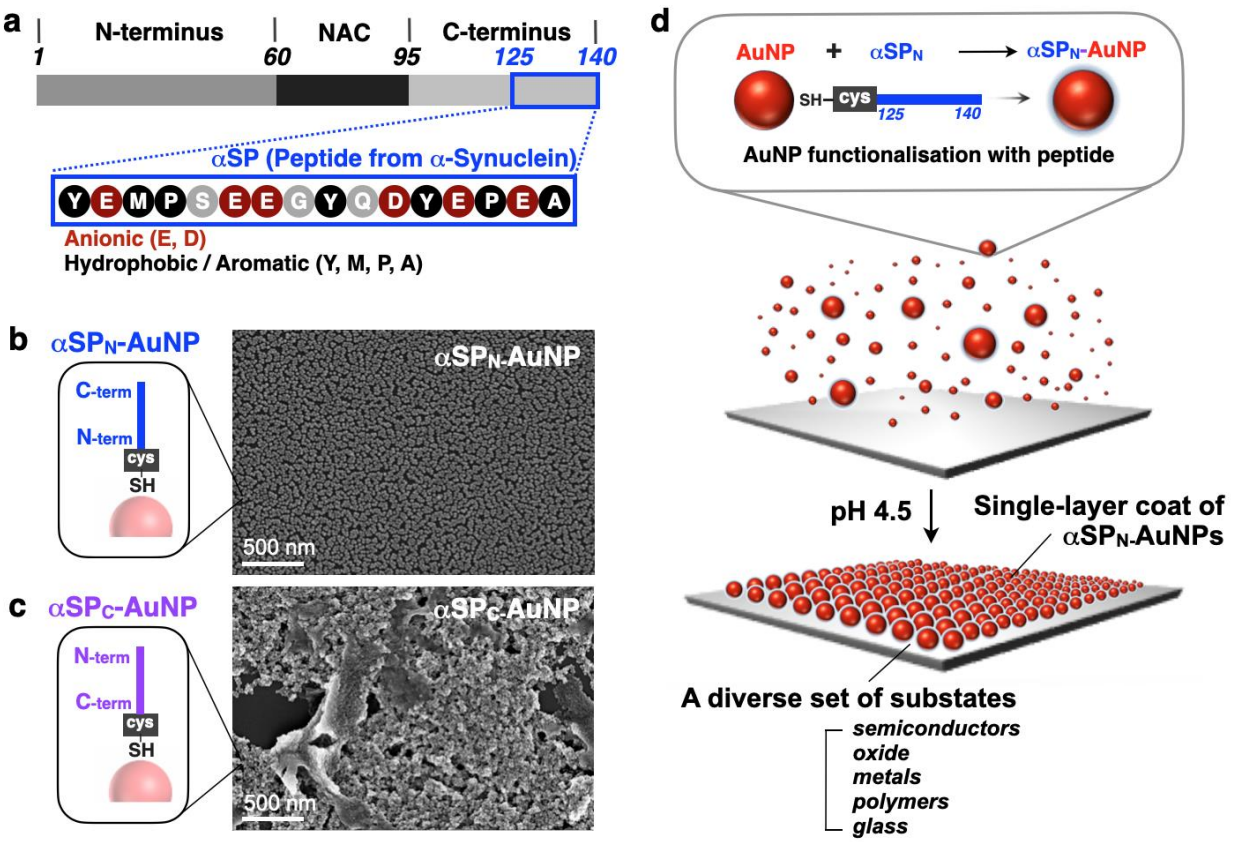

Figure 1. αSP_N and its conjugation with AuNPs to adhere onto substrates. (a) Amino acid sequence of αSP (blue box) located in C-terminal region of αS protein (anionic amino acids in red and hydrophobic/aromatic in black). Conjugation of AuNP with either (b) αSP_N (blue) or (c) αSP_C (purple). SEM images of each conjugate deposited onto silicon wafer after incubation at pH 4.5 (in 50 mM citrate at 40°C for 3hr) are presented. (d) Schematic representation for high-density single layer adhesion of αSP_N-AuNPs onto a diverse set of substrates by acidification to pH 4.5.

protein in the formation of the SNARE complex[28] and the αS-AuNP conjugates.[1,2] Control experiments with AuNPs conjugated with a purely anionic control peptide, composed of a N-terminal cysteine and 6 glutamate residues (CEEEEEE-NH_2; $6E_N$), resulted in a well-dispersed colloidal state of the conjugates (Fig. S1c), which however did not show single layer adsorption and randomly agglomerated on the silicon surface after acidification (Fig. S7).

pH-controlled close-packed single layer adhesion of αSP_N-AuNPs. The adsorption of αSP_N-AuNPs onto the silicon substrate was studied in detail by adjusting the pH, ranging from 3.75 to 4.75 at intervals of 0.25 (Fig. 2a, see supporting information). At the most acidic pH of 3.75, the strong degree of protonation of peptide carboxylates triggered the amorphous agglomeration of the conjugates onto the silicon surface. The typical red wine plasmon color of colloidal AuNPs of the conjugates instantaneously turned dark blue and no material was adsorbed on the pipette tip, which indicated uncontrolled aggregation of the particles (Fig. S8). A sparse monolayer with local agglomerations of the particles was observed at pH 4.00 and pH 4.25. The high-density single layer of αSP_N-AuNPs was obtained at the optimal pH value of 4.50 and a slight decrease of particle density was found at pH 4.75. The detailed analysis of the SEM images allowed precise quantification of the particle density, given in number of particles per µm square (Fig 2b for a statistical analysis see Fig. S9). Calculation of the pI by using the algorithm #[ref] lead to an approximate value of of 3.36, in agreement with a 17 amino acid peptide bearing 6 carboxylates (see supporting information). Therefore, at the pH near the pI (i.e. 3.75), the strong self-associative propensity of the neutralized peptide triggered fast particle-particle amorphous association (Fig. 2c). In contrast, the excellent close packing achieved at pH 4.5 could be rationalized by the balanced surface charge of αSP_N-AuNPs that allowed the particles to be in close proximity with minimum repulsion and without aggregation. As expected, above pH 4.75, the packing was sparse with higher negative charges that make the particles more repulsive (Fig. S10).

Primary structural parameters determining the adhesion properties of αSP_N. To study in detail the length of the adhesive peptide sequence, we prepared serially truncated peptides of αSP_N by removing every two amino acids from the N-terminus of αSP_N (Table S1, αSP_N truncation). After conjugation with AuNPs and deposition onto silicon surfaces, we observed that these sequences were able to achieve certain degree of monolayers surface adhesion (Fig. S11 and 12). However, the shorter peptides resulted in the lower surface coverage (i.e. approximately 35-45% for $_{(4)}\alpha SP_N$-$_{(8)}\alpha SP_N$, and 55-65% for $_{(10)}\alpha SP_N$-αSP_N). The 17 amino acid peptide sequence (αSP_N-AuNP) exhibited the highest NP density (Fig. 3). Next, we studied the impact in the peptide sequence of the proline and the tyrosine amino acids, which have been confirmed in several important

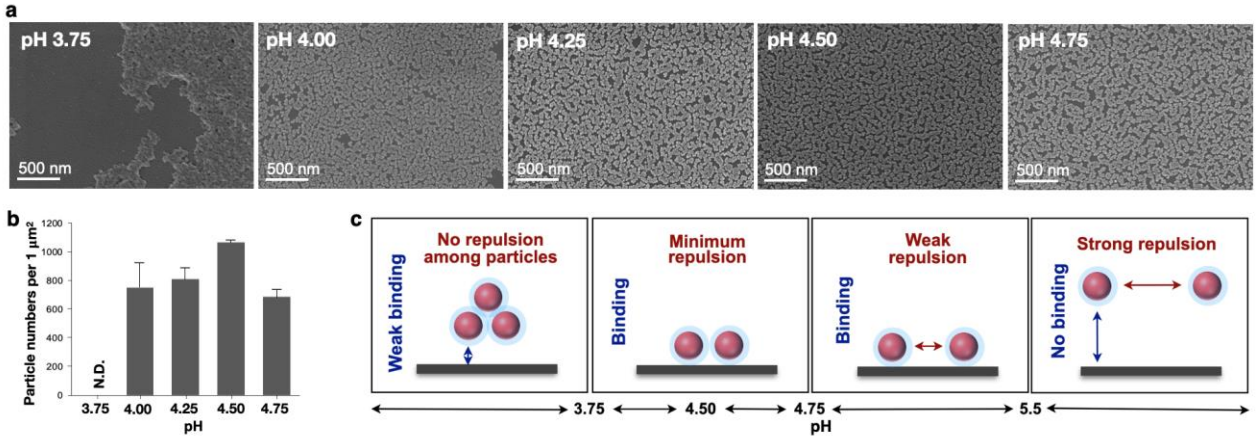

Figure 2. pH-Dependent single-layer adsorption of αSP_N-AuNPs. (a) SEM images of the conjugates on silicon surface after incubation at 40°C for 3 hours in 50 mM citrate at various pHs of 3.75, 4.00, 4.25, 4.50, and 4.75. (b) Packing densities of αSP_N-AuNPs adsorbed onto the surface at different pHs. The density was obtained by counting particles of 3 different independent images (1 μm x 1 μm) (c) Schematic drawings for a model of pH-dependent interplay between binding propensity (particles-surface) and charge repulsion (particles-particles) regarding single-layer adhesion of the conjugates and their organization.

adhesive proteins (e.g. proline-rich proteins, curli fibers).[59-61] The mutant sequences were prepared by replacing Tyr and/or Pro by Ala (Table S1, αSP_N mutants). Adhesion of their NP conjugates onto silicon surfaces evidenced poor coverage and aggregation propensity in comparison with αSP_N (Figure S13 and 14), indicating that Tyr and Pro amino acids were critical for adhesion properties.

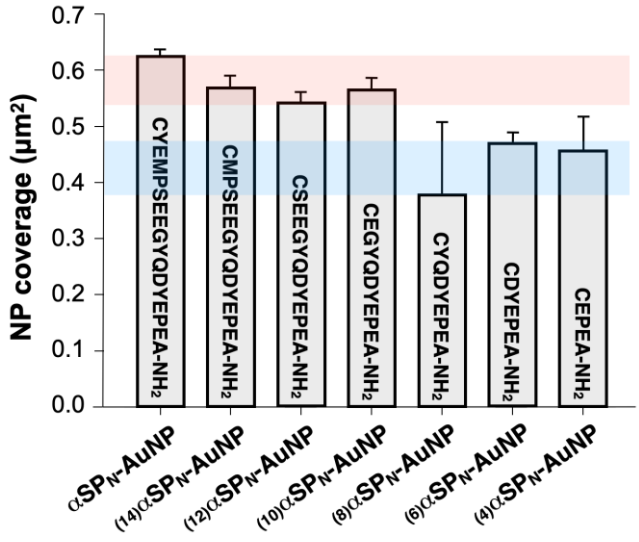

Figure 3. Surface coverage per μm^2 of AuNPs conjugated with serially truncated αSP_N adsorbed onto silicon substrate. The high coverage values of NPs with αSP_N, $_{(14)}\alpha SP_N$, $_{(12)}\alpha SP_N$, and $_{(10)}\alpha SP_N$ are indicated in red, and the low coverage values of NPs with $_{(8)}\alpha SP_N$, $_{(6)}\alpha SP_N$, and $_{(4)}\alpha SP_N$ are marked in blue.

Versatile adsorption of αSP_N-AuNPs onto multiple substrates. The adhesion of the peptide/NP conjugates (αSP_N-AuNP) was tested on a diverse range of substrates. Remarkably, after incubation at pH 4.5, we confirmed that the tightly packed single layer of particles efficiently and homogenously distributed onto a range of materials of different chemical nature such as semiconductors (Si, boron-doped p-type Si), oxide (SiO_2), metals (Au, Ti), glass and polymers (PC, PET) (Fig. 4a and S15a). AFM micrographs (Fig. 4b and S16) and their height profiles (Fig. 4c) revealed the close-packed monolayer adhesion of αSP_N-AuNP with a thickness of about 20 nm that is identical to the diameter of the particles. Intriguingly, when mica was used as a substrate, we observed perfectly crystalline superlattices of the αSP_N-AuNP conjugates adsorbed on the mica surface (Fig. 4d). The AFM analyses showed that the thickness of the superlattice is consistent with the diameter of the AuNPs (Fig 4e and f). In this case, the repulsion with the negatively charged mica surface gives the conjugates a higher mobility on the surface and thus allows a better packing of the particles into superlattices. This observation is supported by the inverse dependence of the optimal pH with the temperature for superlattice formation (Fig. S17). Importantly, the extended single-layer superlattices cannot be achieved with full proteins or other synthetic polymers due to the steric constraints, which are intrinsic to high molecular weight bio-adhesive molecules.[62]

We hypothesized that surface adhesion could be correlated with the chaperone activity of αSP. To investigate this, we used as control a tandem sequence ($_{(tdm)}\alpha SP$, Table S1) that is found in the C-terminal region of αS (109-124). Although its charge distribution is equivalent (Fig. S18), $_{(tdm)}\alpha SP$ has been reported to provide much lower protection against protein denaturation than the αS protein[42]. To evaluate chaperone activity, either αSP or $_{(tdm)}\alpha SP$ were co-incubated with alcohol dehydrogenase (ADH) at 60°C. In this assay, the higher the peptide chaperone activity the more dehydrogenase activity is protected. αSP prevented the loss of ADH activity to retain approximately 85%, which is comparable to the protection by αS protein (~90%), whereas in the presence of the tandem peptide $_{(tdm)}\alpha SP$ the activity was strongly reduced up to ~35% (Fig. 5a). In addition, the chaperone activity of αSP was also confirmed to be higher than $_{(tdm)}\alpha SP$ by the turbidity assays that monitor protein aggregation (ADH and lysozyme) upon heat treatment in the presence of either peptide (Fig. S19). In order to estimate its adhesive capabilities, $_{(tdm)}\alpha S$ was conjugated to AuNP in different orien-

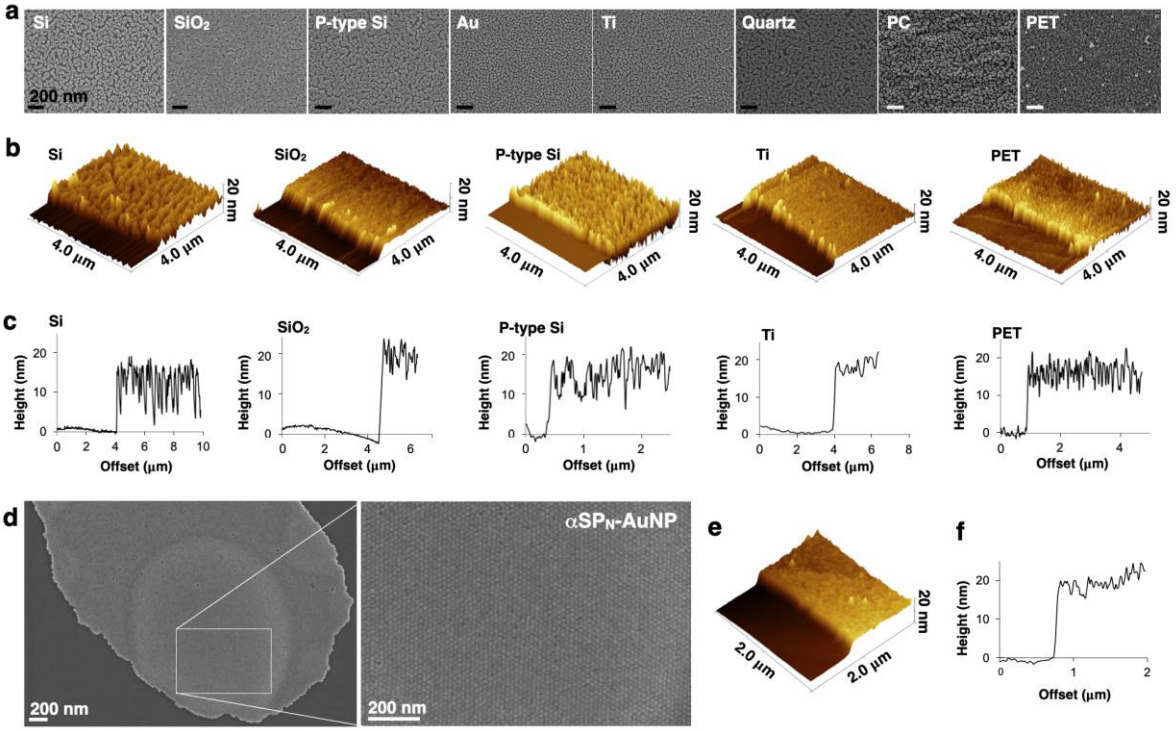

Figure 4. Single-layer coating of αSP_N-AuNPs on multiple substrates. (a) SEM images of the monolayer adhered onto various types of substrates such as Si, SiO_2, boron-doped p-type Si, Au, Ti, quartz, PC, and PET. (b) AFM 3-D images and (c) their height profiles of the single layer on different substrates of Si, SiO_2, boron-doped p-type Si, Ti, and PET. (d) SEM image of the αSP_N-AuNP superlattice on mica surface after incubation at pH 4.5 for 3 hours at 35°C. Area indicated with white-lined box is magnified into the right panel to show detailed superlattice morphology. (e) AFM 3-D and (f) height profile of the superlattice monolayer.

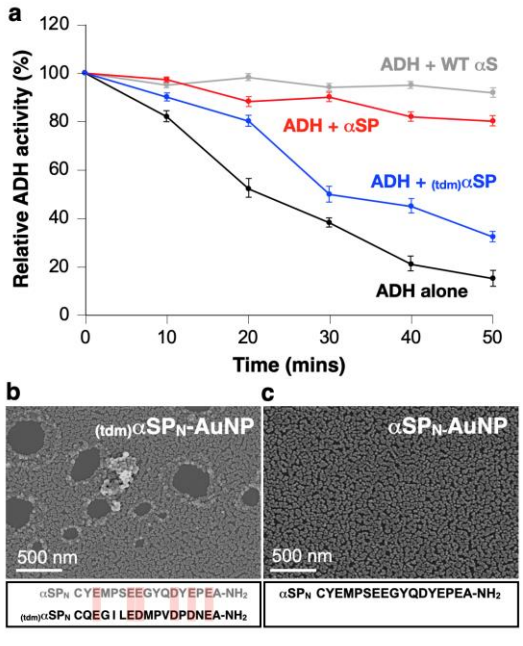

Figure 5. (a) Chaperone function of αSP comparing to $_{(tdm)}$αSP. Chaperone activity was accessed with protection of ADH activity by co-incubating ADH with either αSP (red) or $_{(tdm)}$αSP (blue) during thermal treatment at 60°C for 50 min. Thermal protection of ADH activity in the absence (black) and presence (gray) of αS protein was provided as a control. SEM images of (b) $_{(tdm)}\alpha SP_N$-AuNPs and (c) αSP_N-AuNPs adsorbed onto silicon surface.

tations as described for αSP ($_{((tdm)}\alpha SP_N$ and $_{(tdm)}\alpha SP_C$). After deposition on silicon surfaces, SEM micrographs revealed lower coverages of $_{(tdm)}\alpha SP_{N\text{-}Au}NP$ (Fig. 5b, Fig. S20-21) in comparison to αSP_N-AuNP (Fig. 5c). Moreover, the former showed noticeable vacant areas and nanoparticle agglomerations. This was evidenced across multiple surfaces (Fig. S15b).

Spectroscopic and Structural Characterization. Circular dichroism spectra (CD) indicated that this peptide sequence (αSP_N) had mainly a polyproline II conformation, which is characterized by a minimum around 205 nm and a maximum around 228 nm[63] (Fig. S22). No major conformational rearrangements were observed in the pH range relevant to this study. To confirm the polyproline II character of the peptide, we used NMR to measure the secondary ^{13}C chemical shifts ($\Delta\delta C^{\alpha}$ - $\Delta\delta C^{\beta}$). Along the sequence and over a wide pH range, values are within ±1 ppm (Fig S23a and b). In combination with the CD data they are indicative of polyproline II folding The full αS protein has only 5 prolines[64] and 4 tyrosines[65] in its total sequence of 140 residues. Importantly, most of these residues (all the prolines and 3 tyrosines) are located at the C-terminus, which has been assigned to the binding region of the αS protein. Proline has been found to exhibit promiscuous binding properties in proline-rich proteins (PRPs) such as salivary proteins, mucins, actin-binding proteins, RNA polymerase II, and synapsin I.[59] Additionally, the polar aromatic chemical nature of tyrosine has also been identified in proteins that strongly adhere to different surfaces,[60] and L-dopa/polydopamine was proposed as a multiple coating agent.[18,61] Control experiments with the inverted natural protein sequence from N- to C-terminal (αSP_C), the peptide lacking proline and/or tyrosine ($_{(P\to A)}\alpha SP_N$ and $_{(Y\to A)}\alpha SP_N$), a

tandem peptide ($_{(tdm)}\alpha SP_N$), and a purely anionic peptide containing 6 glutamates residues ($6E_N$) confirmed that the presence and orientation of the tyrosine and the proline residues of the peptide were important to promote the homogenous single layer NP adsorption. NMR analysis of the side chain chemical shifts allowed the calculation of the individual pKas of each of the carboxylates of this peptide sequence (Fig. S23). The pKa range oscillated between 4.2 and 5.0, which confirmed that around 50% of the carboxylates would be deprotonated at the optimal pH for particle adhesion. This partial reduction of the anionic character of the peptide is likely sufficient to enhance the van der Walls and the hydrophobic interactions of the three tyrosines and the two prolines present in the short peptide sequence described here (i.e. **Y**EM**P**SEEG**Y**QD**Y**E**P**EA). Therefore, partial protonation of the carboxylates in the glutamic and aspartic residues leads to a dramatic enhancement of their surface affinity.[66]

Conclusions

The objective of this work was to identify a short peptide sequence that could retain the intriguing adhesive properties of the αS but lacking the synthetic and size limitations intrinsic to the full protein. The peptide sequence described here corresponding to the C-terminal region of αS, αSP_N, is composed of only 17 amino acids including 6 negatively charged carboxylate residues, which partial protonation triggered homogenous adhesion of AuNPs and even crystalline superlattices. This peptide functions as a versatile adhesive agent for the guided adsorption of a tightly packed single layer of NPs onto a range of different substrates. Peptide/particle surface binding resulted in a homogenous large area adhesion of high-density and even crystalline monolayers of NPs. The peptide sequence discovered here goes beyond the synthetic and size limitations of other biocompatible strategies using full protein linkers. Altogether, the results described here suggested that the C-terminal region from residue 125-140 of αS can be responsible for the pluripotent adsorption capacity of αS. Furthermore, the discovery of this short peptide could assist in the general potential exploitation of the physiological adhesive properties and the chaperone activity of αS.

ASSOCIATED CONTENT

Supporting Information

The Supporting Information is available free of charge on the ACS Publications website.

AUTHOR INFORMATION

Corresponding Author

* Javier Montenegro, PhD., e-mail: javier.montenegro@usc.es

ACKNOWLEDGMENT

This work was partially supported by the Spanish Agencia Estatal de Investigación (AEI) [BIO2015-70092-R, SAF2017-89890-R], the Xunta de Galicia (ED431C 2017/25, 2016-AD031, AGAUR (2017 SGR 324), and Centro Singular de Investigación de Galicia accreditation 2016–2019, ED431G/09), the ISCIII (RD16/0008/003), and the European Union (European Regional Development Fund – ERDF). X.S. acknowledges funding from the ERC (CONCERT-648201). IRB Barcelona is the recipient of a Severo Ochoa Award (Government of Spain). J.M. received a Ramón y Cajal (RYC-2013-13784), an ERC Starting Grant (DYNAP-677786) and a Young Investigator Grant from the HFSP (RGY0066/2017).

REFERENCES

(1) Aricò, A. S.; Bruce, P.; Scrosati, B.; Tarascon, J. M.; Van Schalkwijk, W. Nanostructured Materials for Advanced Energy Conversion and Storage Devices. *Nat. Mater.* **2005**, *4*, 366–377.

(2) Willets, K. A.; Van Duyne, R. P. Localized Surface Plasmon Resonance Spectroscopy and Sensing. *Annu. Rev. Phys. Chem.* **2007**, *58*, 267–297.

(3) Atwater, H. A.; Polman, A. Plasmonics for Improved Photovoltaic Devices. *Nat. Mater.* **2010**, *9*, 205–213.

(4) Han, S. T.; Zhou, Y.; Xu, Z. X.; Huang, L. B.; Yang, X. B.; Roy, V. A. L. Microcontact Printing of Ultrahigh Density Gold Nanoparticle Monolayer for Flexible Flash Memories. *Adv. Mater.* **2012**, *24*, 3556–3561.

(5) Kuan, S. L.; Bergamini, F. R. G.; Weil, T. Functional Protein Nanostructures: a Chemical Toolbox. *Chem. Soc. Rev.* **2018**, *47*, 9069–9105.

(6) Shipway, A. N.; Katz, E.; Willner, I. Nanoparticle Arrays on Surfaces for Electronic, Optical, and Sensor Applications. *ChemPhysChem* **2000**, *1*, 18–52.

(7) Malynych, S.; Luzinov, I.; Chumanov, G. Poly(Vinyl Pyridine) as a Universal Surface Modifier for Immobilization of Nanoparticles. *J. Phys. Chem. B* **2002**, *106*, 1280–1285.

(8) Sainsbury, T.; Ikuno, T.; Okawa, D.; Pacilé, D.; Fréchet, J. M. J.; Zettl, A. Self-Assembly of Gold Nanoparticles at the Surface of Amine- and Thiol-Functionalized Boron Nitride Nanotubes. *J. Phys. Chem. C* **2007**, *111*, 12992–12999.

(9) Moyano, D. F.; Liu, Y.; Ayaz, F.; Hou, S.; Puangploy, P.; Duncan, B.; Osborne, B. A.; Rotello, V. M. Immunomodulatory Effects of Coated Gold Nanoparticles in LPS-Stimulated in Vitro and in Vivo Murine Model Systems. *Chem* **2016**, *1*, 320–327.

(10) Cheng, W.; Campolongo, M. J.; Cha, J. J.; Tan, S. J.; Umbach, C. C.; Muller, D. A.; Luo, D. Free-Standing Nanoparticle Superlattice Sheets Controlled by DNA. *Nat. Mater.* **2009**, *8*, 519–525.

(11) Macfarlane, R. J.; Lee, B.; Jones, M. R.; Harris, N.; Schatz, G. C.; Mirkin, C. A. Nanoparticle Superlattice Engineering with DNA. *Science* **2011**, *334*, 204–208.

(12) McMillan, R. A.; Paavola, C. D.; Howard, J.; Chan, S. L.; Zaluzec, N. J.; Trent, J. D. Ordered Nanoparticle Arrays Formed on Engineered Chaperonin Protein Templates. *Nat. Mater.* **2002**, *1*, 247–252.

(13) Bhak, G.; Lee, J.; Kim, C. H.; Chung, D. Y.; Kang, J. H.; Oh, S.; Lee, J.; Kang, J. S.; Yoo, J. M.; Yang, J. E.; *et al.* High-Density Single-Layer Coating of Gold Nanoparticles Onto Multiple Substrates by Using an Intrinsically Disordered Protein of α-Synuclein for Nanoapplications. *ACS Appl. Mater. Interfaces* **2017**, *9*, 8519–8532.

(14) van Dongen, S. F. M.; de Hoog, H. P. M.; Peters, R. J. R. W.; Nallani, M.; Nolte, R. J. M.; van Hest, J. C. M. Biohybrid Polymer Capsules. *Chem. Rev.* **2009**, *109*, 6212–6274.

(15) Chakraborty, I.; Parak, W. J. Protein-Induced Shape Control of Noble Metal Nanoparticles. *Adv. Mater. Interfaces* **2019**, *6*, 1801407–1801407.

(16) Aires, A.; Llarena, I.; Moller, M.; Castro-Smirnov, J.; Cabanillas-Gonzalez, J.; Cortajarena, A. L. A Simple

Approach to Design Proteins for the Sustainable Synthesis of Metal Nanoclusters. *Angew. Chem. Int. Ed.* **2019**, *58*, 6214–6219.

(17) Dominguez-Medina, S.; Kisley, L.; Tauzin, L. J.; Hoggard, A.; Shuang, B.; D S Indrasekara, A. S.; Chen, S.; Wang, L. Y.; Derry, P. J.; Liopo, A.; *et al.* Adsorption and Unfolding of a Single Protein Triggers Nanoparticle Aggregation. *ACS Nano* **2016**, *10*, 2103–2112.

(18) Lee, H.; Dellatore, S. M.; Miller, W. M.; Messersmith, P. B. Mussel-Inspired Surface Chemistry for Multifunctional Coatings. *Science* **2007**, *318*, 426–430.

(19) Ryou, M. H.; Kim, J.; Lee, I.; Kim, S.; Jeong, Y. K.; Hong, S.; Ryu, J. H.; Kim, T. S.; Park, J. K.; Lee, H.; *et al.* Mussel-Inspired Adhesive Binders for High-Performance Silicon Nanoparticle Anodes in Lithium-Ion Batteries. *Adv. Mater.* **2013**, *25*, 1571–1576.

(20) Ku, S. H.; Lee, J. S.; Park, C. B. Spatial Control of Cell Adhesion and Patterning Through Mussel-Inspired Surface Modification by Polydopamine. *Langmuir* **2010**, *26*, 15104–15108.

(21) You, I.; Lee, T. G.; Nam, Y. S.; Lee, H. Fabrication of a Micro-Omnifluidic Device by Omniphilic/Omniphobic Patterning on Nanostructured Surfaces. *ACS Nano* **2014**, *8*, 9016–9024.

(22) Zhu, Q.; Pan, Q. Mussel-Inspired Direct Immobilization of Nanoparticles and Application for Oil-Water Separation. *ACS Nano* **2014**, *8*, 1402–1409.

(23) Islam, M. S.; Akter, N.; Rahman, M. M.; Shi, C.; Islam, M. T.; Zeng, H.; Azam, M. S. Mussel-Inspired Immobilization of Silver Nanoparticles Toward Antimicrobial Cellulose Paper. *ACS Sustainable Chemistry and Engineering* **2018**, *6*, 9178–9188.

(24) Lee, J.; Bhak, G.; Lee, J. H.; Park, W.; Lee, M.; Lee, D.; Jeon, N. L.; Jeong, D. H.; Char, K.; Paik, S. R. Free-Standing Gold-Nanoparticle Monolayer Film Fabricated by Protein Self-Assembly of α-Synuclein. *Angew. Chem. Int. Ed.* **2015**, *54*, 4571–4576.

(25) Yang, J. A.; Johnson, B. J.; Wu, S.; Woods, W. S.; George, J. M.; Murphy, C. J. Study of Wild-Type α-Synuclein Binding and Orientation on Gold Nanoparticles. *Langmuir* **2013**, *29*, 4603–4615.

(26) Richman, M.; Wilk, S.; Chemerovski, M.; Wärmländer, S. K. T. S.; Wahlström, A.; Gräslund, A.; Rahimipour, S. In Vitro and Mechanistic Studies of an Antiamyloidogenic Self-Assembled Cyclic D, L-A-Peptide Architecture. *J. Am. Chem. Soc.* **2013**, *135*, 3474–3484.

(27) Spillantini, M. G.; Schmidt, M. L.; Lee, V. M. Y.; Trojanowski, J. Q.; Jakes, R.; Goedert, M. α-Synuclein in Lewy Bodies. *Nature* **1997**, *388*, 839–840.

(28) Burré, J.; Sharma, M.; Tsetsenis, T.; Buchman, V.; Etherton, M. R.; Südhof, T. C. α-Synuclein Promotes SNARE-Complex Assembly in Vivo and in Vitro. *Science* **2010**, *329*, 1663–1667.

(29) Deleersnijder, A.; Gerard, M.; Debyser, Z.; Baekelandt, V. The Remarkable Conformational Plasticity of Alpha-Synuclein: Blessing or Curse? *Trends Mol. Med.* **2013**, *19*, 368–377.

(30) Wright, P. E.; Dyson, H. J. Intrinsically Disordered Proteins in Cellular Signalling and Regulation. *Nat. Rev. Mol. Cell. Bio.* **2015**, *16*, 18–29.

(31) Ullman, O.; Fisher, C. K.; Stultz, C. M. Explaining the Structural Plasticity of α-Synuclein. *J. Am. Chem. Soc.* **2011**, *133*, 19536–19546.

(32) Davidson, W. S.; Jonas, A.; Clayton, D. F.; George, J. M. Stabilization of α-Synuclein Secondary Structure Upon Binding to Synthetic Membranes. *J. Biol. Chem.* **1998**, *273*, 9443–9449.

(33) Ueda, K.; Fukushima, H.; Masliah, E.; Xia, Y.; Iwai, A.; Yoshimoto, M.; Otero, D. A. C.; Kondo, J.; Ihara, Y.; Saitoh, T. Molecular Cloning of cDNA Encoding an Unrecognized Component of Amyloid in Alzheimer Disease. *Proc. Natl. Acad. Sci. U. S. A.* **1993**, *90*, 11282–11286.

(34) Hoyer, W.; Cherny, D.; Subramaniam, V.; Jovin, T. M. Impact of the Acidic C-Terminal Region Comprising Amino Acids 109−140 on α-Synuclein Aggregation in Vitro. *Biochemistry* **2004**, *43*, 16233–16242.

(35) Jao, C. C.; Der-Sarkissian, A.; Chen, J.; Langen, R. Structure of Membrane-Bound α-Synuclein Studied by Site-Directed Spin Labeling. *Proc. Natl. Acad. Sci. U. S. A.* **2004**, *101*, 8331–8336.

(36) Wietek, J.; Haralampiev, I.; Amoussouvi, A.; Herrmann, A.; Stöckl, M. Membrane Bound α-Synuclein Is Fully Embedded in the Lipid Bilayer While Segments with Higher Flexibility Remain. *FEBS Lett* **2013**, *587*, 2572–2577.

(37) Der-Sarkissian, A.; Jao, C. C.; Chen, J.; Langen, R. Structural Organization of α-Synuclein Fibrils Studied by Site-Directed Spin Labeling. *J. Biol. Chem.* **2003**, *278*, 37530–37535.

(38) Park, S. M.; Jung, H. Y.; Chung, K. C.; Rhim, H.; Park, J. H.; Kim, J. Stress-Induced Aggregation Profiles of GST−α-Synuclein Fusion Proteins: Role of the C-Terminal Acidic Tail of Alpha-Synuclein in Protein Thermosolubility and Stability. *Biochemistry* **2002**, *41*, 4137–4146.

(39) Kim, T. D.; Paik, S. R.; Yang, C. H.; Kim, J. Structural Changes in α-Synuclein Affect Its Chaperone-Like Activity in Vitro. *Protein Sci.* **2000**, *9*, 2489–2496.

(40) Souza, J. M.; Giasson, B. I.; Lee, V. M. Y.; Ischiropoulos, H. Chaperone-Like Activity of Synucleins. *FEBS Lett* **2000**, *474*, 116–119.

(41) Park, S. M.; Jung, H. Y.; Kim, T. D.; Park, J. H.; Yang, C. H.; Kim, J. Distinct Roles of the N-Terminal-Binding Domain and the C-Terminal-Solubilizing Domain of α-Synuclein, a Molecular Chaperone. *J. Biol. Chem.* **2002**, *277*, 28512–28520.

(42) Kim, T. D.; Paik, S. R.; Yang, C. H. Structural and Functional Implications of C-Terminal Regions of α-Synuclein. *Biochemistry* **2002**, *41*, 13782–13790.

(43) Fujiwara, H.; Hasegawa, M.; Dohmae, N.; Kawashima, A.; Masliah, E.; Goldberg, M. S.; Shen, J.; Takio, K.; Iwatsubo, T. α-Synuclein Is Phosphorylated in Synucleinopathy Lesions. *Nat Cell Biol* **2002**, *4*, 160–164.

(44) Giasson, B. I.; Duda, J. E.; Murray, I. V. J.; Chen, Q.; Souza, J. M.; Hurtig, H. I.; Ischiropoulos, H.; Trojanowski, J. Q.; Lee, V. M. Y. Oxidative Damage Linked to Neurodegeneration by Selective α-Synuclein Nitration in Synucleinopathy Lesions. *Science* **2000**, *290*, 985–989.

(45) Giasson, B. I.; Forman, M. S.; Higuchi, M.; Golbe, L. I.; Graves, C. L.; Kotzbauer, P. T.; Trojanowski, J. Q.; Lee, V. M. Y. Initiation and Synergistic Fibrillization of Tau and Alpha-Synuclein. *Science* **2003**, *300*, 636–640.

(46) Paik, S. R.; Lee, D.; Cho, H. J.; Lee, E. N.; Chang, C. S. Oxidized Glutathione Stimulated the Amyloid Formation of α-Synuclein. *FEBS Lett* **2003**, *537*, 63–67.

(47) Lee, E. N.; Cho, H. J.; Lee, C. H.; Lee, D.; Chung, K. C.; Paik, S. R. Phthalocyanine Tetrasulfonates Affect the Amyloid Formation and Cytotoxicity of α-Synuclein. *Biochemistry* **2004**, *43*, 3704–3715.

(48) Shin, H. J.; Lee, E. K.; Lee, J. H.; Lee, D.; Chang, C. S.; Kim, Y. S.; Paik, S. R. Eosin Interaction of α-Synu-

clein Leading to Protein Self-Oligomerization. *Biochim. Biophys. Acta* **2000**, *1481*, 139–146.
(49) Lee, C. H.; Kim, H. J.; Lee, J. H.; Cho, H. J.; Kim, J.; Chung, K. C.; Jung, S.; Paik, S. R. Dequalinium-Induced Protofibril Formation of α-Synuclein. *J. Biol. Chem.* **2006**, *281*, 3463–3472.
(50) Bertoncini, C. W.; Jung, Y. S.; Fernandez, C. O.; Hoyer, W.; Griesinger, C.; Jovin, T. M.; Zweckstetter, M. Release of Long-Range Tertiary Interactions Potentiates Aggregation of Natively Unstructured α-Synuclein. *Proc. Natl. Acad. Sci. U. S. A.* **2005**, *102*, 1430–1435.
(51) McClendon, S.; Rospigliosi, C. C.; Eliezer, D. Charge Neutralization and Collapse of the C-Terminal Tail of Alpha-Synuclein at Low pH. *Protein Science* **2009**, *18*, 1531–1540.
(52) Lv, Z.; Krasnoslobodtsev, A. V.; Zhang, Y.; Ysselstein, D.; Rochet, J. C.; Blanchard, S. C.; Lyubchenko, Y. L. Effect of Acidic pH on the Stability of α-Synuclein Dimers. *Biopolymers* **2016**, *105*, 715–724.
(53) Cole, N. B.; DiEuliis, D.; Leo, P.; Mitchell, D. C.; Nussbaum, R. L. Mitochondrial Translocation of α-Synuclein Is Promoted by Intracellular Acidification. *Exp. Cell. Res.* **2008**, *314*, 2076–2089.
(54) Tapley, T. L.; Körnera, J. L.; Barge, M. T.; Hupfeld, J.; Schauerte, J. A.; Gafni, A.; Jakob, U.; Bardwell, J. C. A. Structural Plasticity of an Acid-Activated Chaperone Allows Promiscuous Substrate Binding. *Proc. Natl. Acad. Sci. U. S. A.* **2009**, *106*, 5557–5562.
(55) Ashcroft, A. E.; Brinker, A.; Coyle, J. E.; Weber, F.; Kaiser, M.; Moroder, L.; Parsons, M. R.; Jager, J.; Hartl, U. F.; Hayer-Hartl, M.; *et al.* Structural Plasticity and Noncovalent Substrate Binding in the GroEL Apical Domain. *J. Biol. Chem.* **2002**, *277*, 33115–33126.
(56) Hu, K.; Galius, V.; Pervushin, K. Structural Plasticity of Peptidyl−Prolyl Isomerase sFkpA Is a Key to Its Chaperone Function as Revealed by Solution NMR. *Biochemistry* **2006**, *45*, 11983–11991.
(57) Lostalé-Seijo, I.; Louzao, I.; Juanes, M.; Montenegro, J. Peptide/Cas9 Nanostructures for Ribonucleoprotein Cell Membrane Transport and Gene Edition. *Chem. Sci.* **2017**, 8, 7923-7931.
(58) Pazo, M.; Juanes, M.; Lostalé-Seijo, I.; Montenegro, J. Oligoalanine Helical Callipers for Cell Penetration. *Chem. Commun.* **2018**, *54*, 6919–6922.
(59) Williamson, M. P. The Structure and Function of Proline-Rich Regions in Proteins. *Biochem. J.* **1994**, *297*, 249–260.
(60) DeBenedictis, E. P.; Liu, J.; Keten, S. Adhesion Mechanisms of Curli Subunit CsgA to Abiotic Surfaces. *Sci. Adv.* **2016**, *2*, e1600998.
(61) Lee, H.; Scherer, N. F.; Messersmith, P. B. Single-Molecule Mechanics of Mussel Adhesion. *Proc. Natl. Acad. Sci. U. S. A.* **2006**, *103*, 12999–13003.
(62) Si, K. J.; Chen, Y.; Shi, Q.; Cheng, W. Nanoparticle Superlattices: the Roles of Soft Ligands. *Adv. Sci.* **2018**, 8*5*,1700179.
(63) Rucker, A. L.; Creamer, T. P. Polyproline II helical structure in protein unfolded states: Lysine peptides revisited. *Protein Sci.* **2002**, *11*, 980–985.
(64) Meuvis, J.; Gerard, M.; Desender, L.; Baekelandt, V.; Engelborghs, Y. The Conformation and the Aggregation Kinetics of α-Synuclein Depend on the Proline Residues in Its C-Terminal Region. *Biochemistry* **2010**, *49*, 9345–9352.
(65) Izawa, Y.; Tateno, H.; Kameda, H.; Hirakawa, K.; Hato, K.; Yagi, H.; Hongo, K.; Mizobata, T.; Kawata, Y. Role of C-Terminal Negative Charges and Tyrosine Residues in Fibril Formation of α-Synuclein. *Brain Behav.* **2012**, *2*, 595–605.
(66) Shemetov, A. A.; Nabiev, I.; Sukhanova, A. Molecular Interaction of Proteins and Peptides with Nanoparticles. *ACS Nano* **2012**, *6*, 4585–4602.

TOC graphic

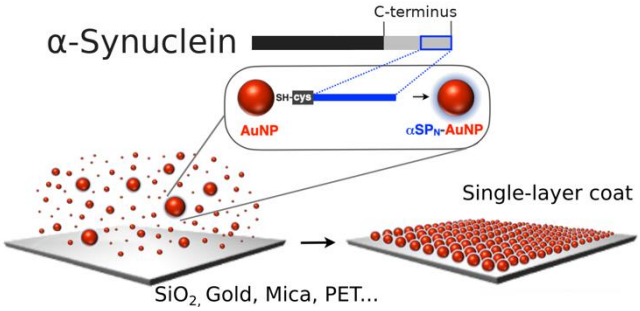
C-terminus
α-Synuclein
SH-Cys
AuNP
αSPN-AuNP
Single-layer coat
SiO2, Gold, Mica, PET...